



Short communication

A novel method for synthesis of layered $\text{LiNi}_{1/3}\text{Mn}_{1/3}\text{Co}_{1/3}\text{O}_2$ as cathode material for lithium-ion battery

Feng Wu, Meng Wang, Yuefeng Su*, Liying Bao, Shi Chen

School of Chemical Engineering and Environment, Beijing Institute of Technology, National Development Center of High Technology Green Materials, Beijing 100081, China

ARTICLE INFO

Article history:

Received 8 July 2009

Received in revised form 8 September 2009

Accepted 15 October 2009

Available online 27 October 2009

Keywords:

Hydrothermal

Cathode

 $\text{LiNi}_{1/3}\text{Mn}_{1/3}\text{Co}_{1/3}\text{O}_2$

Lithium-ion battery

ABSTRACT

The layered $\text{LiNi}_{1/3}\text{Mn}_{1/3}\text{Co}_{1/3}\text{O}_2$ materials with good crystalline are synthesized by a novel method of hydrothermal method followed by a short calcination process. The crystalline structure and morphology of the synthesized materials are characterized by XRD, SEM. Their electrochemical performances are evaluated by CV, EIS and galvanostatic charge/discharge tests. The material synthesized at 850°C for 6 h shows the highest initial discharge capacity of 187.7 mAh g^{-1} at 20 mA g^{-1} . And the capacity retention of 97.9% is maintained at the end of 40 cycles at 1.0 C. CV test reveals almost no shift of anodic and cathodic peaks after first cycle, which indicates good reversible deintercalation and intercalation of Li^+ ions.

© 2009 Elsevier B.V. All rights reserved.

1. Introduction

Recently, the layered $\text{LiNi}_x\text{Mn}_y\text{Co}_{1-x-y}\text{O}_2$ composites have attracted many attentions for their high capacity, good cycling stability and excellent thermal stability [1–4]. Among them, $\text{LiNi}_{1/3}\text{Mn}_{1/3}\text{Co}_{1/3}\text{O}_2$ has shown to be one of the most promising alternative materials in terms of operating voltage, high discharge capacity, high rate capability, cycle-ability, good structural and thermal stability [5–9] and is considered to be one of the best candidates of cathode material for hybrid electric vehicle (HEV) power source system. The electrochemical performance of $\text{LiNi}_{1/3}\text{Mn}_{1/3}\text{Co}_{1/3}\text{O}_2$ is extremely depends on the synthesis method. Because the crystallinity, phase purity, particle morphology, grain size, surface area, and cation distribution in the structure which rely on the synthesis method all play important roles in the electrochemical performance of the material [10,11]. Unfortunately, it is difficult to prepare this complicated compound by using traditional solid state method, because it often result in an inhomogeneous or impure product with lower capacity and poor cycling performance [12–14]. As for sol–gel synthesis method of $\text{LiNi}_{1/3}\text{Mn}_{1/3}\text{Co}_{1/3}\text{O}_2$, high temperature calcination is also necessary to prepare a pure phase, which results in an undesirable particles growth. In this aspect, some researches have reported co-precipitation method to prepare metal hydroxide would be a better method, because the method provides a new approach to

synthesis materials under milder conditions, which offers various morphologies and easy control. But the condition of such reaction must be strictly controlled and quite long reaction time is needed [9]. Hydrothermal treatment is a promising process to improve the crystallinity of transition metal oxide cathode materials. This is because the hydrothermal reaction could be carried out at a low temperature, while under high pressure in a sealed condition. The hydrothermal treatment of hydroxide precursor could greatly improve the electrochemical properties of the cathode materials. Although there are many literature reports about hydroxide co-precipitation, there is little work about hydrothermal treatment of $\text{Ni}_{1/3}\text{Mn}_{1/3}\text{Co}_{1/3}(\text{OH})_2$ to synthesize $\text{LiNi}_{1/3}\text{Mn}_{1/3}\text{Co}_{1/3}\text{O}_2$. This novel method could obtain the product at a relative short time and low calcination temperature. The structure, morphology and electrochemical properties of the prepared $\text{LiNi}_{1/3}\text{Mn}_{1/3}\text{Co}_{1/3}\text{O}_2$ have been investigated in detail.

2. Experimental

$\text{Co}(\text{CH}_3\text{CO}_2)_2 \cdot 4\text{H}_2\text{O}$, $\text{C}_4\text{H}_6\text{MnO}_4 \cdot 4\text{H}_2\text{O}$, $\text{C}_4\text{H}_6\text{NiO}_4 \cdot 4\text{H}_2\text{O}$ as the starting materials were dissolved in deionized water with the mole ratio of 1:1:1. The aqueous solution of acetate was pumped into a continuously stirred reactor. NH_4OH was dripped into the solution at a constant rate till pH 11.0 was reached, and then $\text{LiOH} \cdot \text{H}_2\text{O}$ was slowly added. Such as-prepared suspension (the hydroxides precipitate and the solution) was transferred to a 100 ml Teflon beaker autoclave and filled to 85% of the capacity. The autoclave was sealed and heated at 160°C under auto-generated pressure for 30 h, and then cooled to room temperature naturally. After that, a colorless clear solution and brown precipitate was obtained. The

* Corresponding author. Tel.: +86 10 68918099; fax: +86 10 68918099.
E-mail address: suyuefeng@bit.edu.cn (Y. Su).

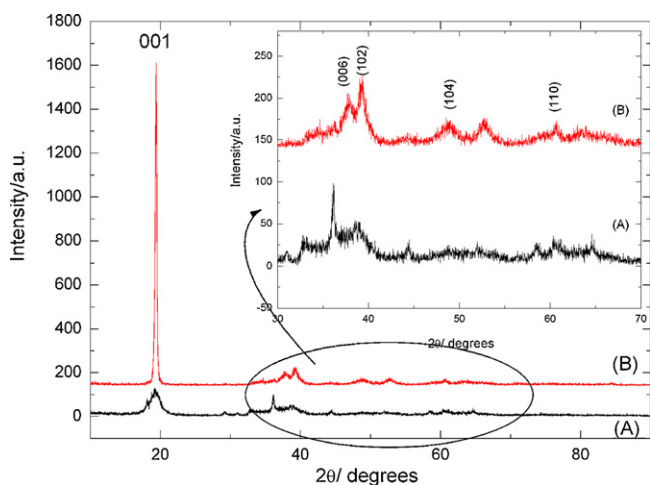


Fig. 1. XRD patterns of $[\text{Ni}_{1/3}\text{Mn}_{1/3}\text{Co}_{1/3}](\text{OH})_2$ (A) before hydrothermal treatment and (B) after hydrothermal treatment.

solution was removed by filtration and the hydrothermal treated hydroxides was washed with deionized water and dried in air at 60°C overnight. The dried precipitate was then grounded with 5% excess $\text{LiOH}\cdot\text{H}_2\text{O}$ (excess amount of $\text{LiOH}\cdot\text{H}_2\text{O}$ was used to compensate possible Li loss during the calcination [15]). The powders were calcined at 850°C by different time in air, viz., 4, 6, 8 and 10 h, respectively. Hereafter, the materials synthesized by 4, 6, 8 and 10 h were referred as A, B, C and D, respectively.

X-ray diffraction (XRD) measurement was carried out using Cu target $K\alpha$ radiation in the 2θ range of $10\text{--}90^\circ$. D Max-RD12Kw diffractometer were used to test the $[\text{Ni}_{1/3}\text{Mn}_{1/3}\text{Co}_{1/3}](\text{OH})_2$ with the steps of 8°min^{-1} ; D Max-RB12Kw diffractometer were used to test $\text{LiNi}_{1/3}\text{Mn}_{1/3}\text{Co}_{1/3}\text{O}_2$ with the steps of 1.2°min^{-1} . The struc-

tural parameters were obtained by the Rietveld refinement method using the FullProf2006 program. Scanning electron microscope (SEM) was performed using QUANTA 600.

The electrochemical properties of $\text{LiNi}_{1/3}\text{Mn}_{1/3}\text{Co}_{1/3}\text{O}_2$ were examined in the CR2025 coin type cells. The cathode electrodes were prepared by pasting the mixture of 85.0 wt.% $\text{LiNi}_{1/3}\text{Mn}_{1/3}\text{Co}_{1/3}\text{O}_2$, 10.0 wt.% acetylene black and 5.0 wt.% PVDF onto a aluminum foil current collector. The electrolyte was 1 M $\text{LiPF}_6/\text{EC} + \text{DMC}$ (1:1 in volume). The cells were assembled in an Argon-filled glove box, then aged for 12 h before electrochemically cycled between 2.8 and 4.5 V (vs. Li/Li^+) using CT2001A Land instrument.

The cyclic voltammogram (CV) was operated at 0.1mVs^{-1} between 2.5 and 4.8 V. The electrochemical impedance spectroscopy (EIS) measurements were conducted by a CHI660a impedance analyzer, using an amplitude voltage 5 mV and frequency range was 0.001–0.1 MHz.

3. Results and discussion

3.1. Structure and morphology

The XRD patterns of $[\text{Ni}_{1/3}\text{Mn}_{1/3}\text{Co}_{1/3}](\text{OH})_2$ before and after hydrothermal treatment with $\text{LiOH}\cdot\text{H}_2\text{O}$ are shown in Fig. 1. It could see that the intensity of precursor B is different from the precursor A. Because that the intensity of reflections is decided by crystal orientation, so it is reasonable to deduce the crystal orientation is different between the two samples. The reflection intensity of precursor B (especially the 003 diffraction patterns) is much higher than that of the precursor A, it means that the crystal orientation of precursor after hydrothermal treatment become higher. In addition, the XRD patterns of the both precursors show broad integrated lines. The broad integrated lines can be attributed to the mixed effects of transition metal hydroxides such as $\text{Mn}(\text{OH})_2$, $\text{Ni}(\text{OH})_2$

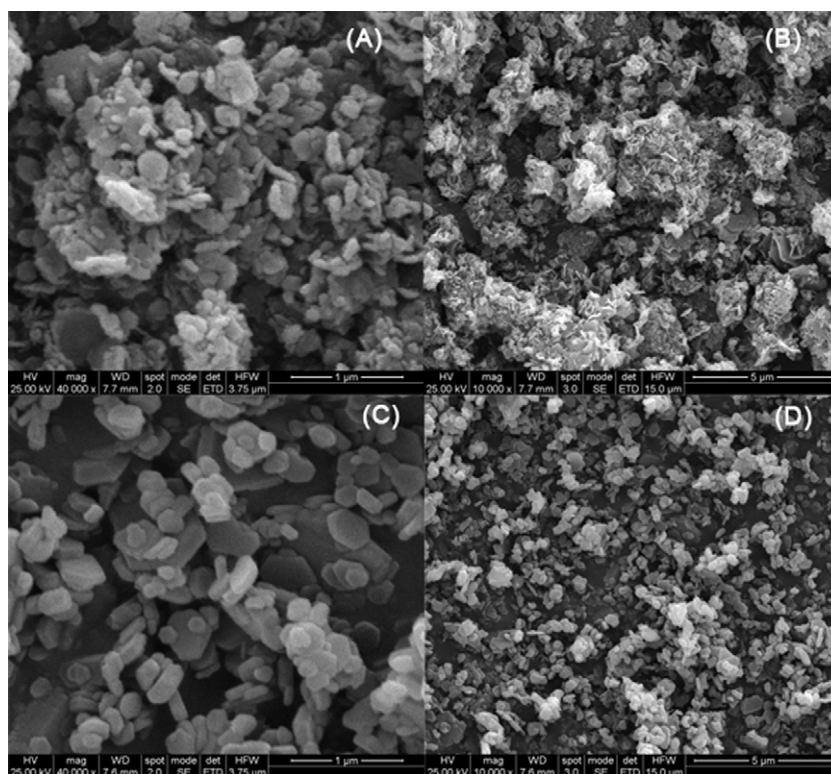


Fig. 2. SEM images of $[\text{Ni}_{1/3}\text{Mn}_{1/3}\text{Co}_{1/3}](\text{OH})_2$ (A) before hydrothermal treatment $40,000\times$, (B) before hydrothermal treatment $10,000\times$, and (C) after hydrothermal treatment $40,000\times$, and (D) after hydrothermal treatment $10,000\times$.

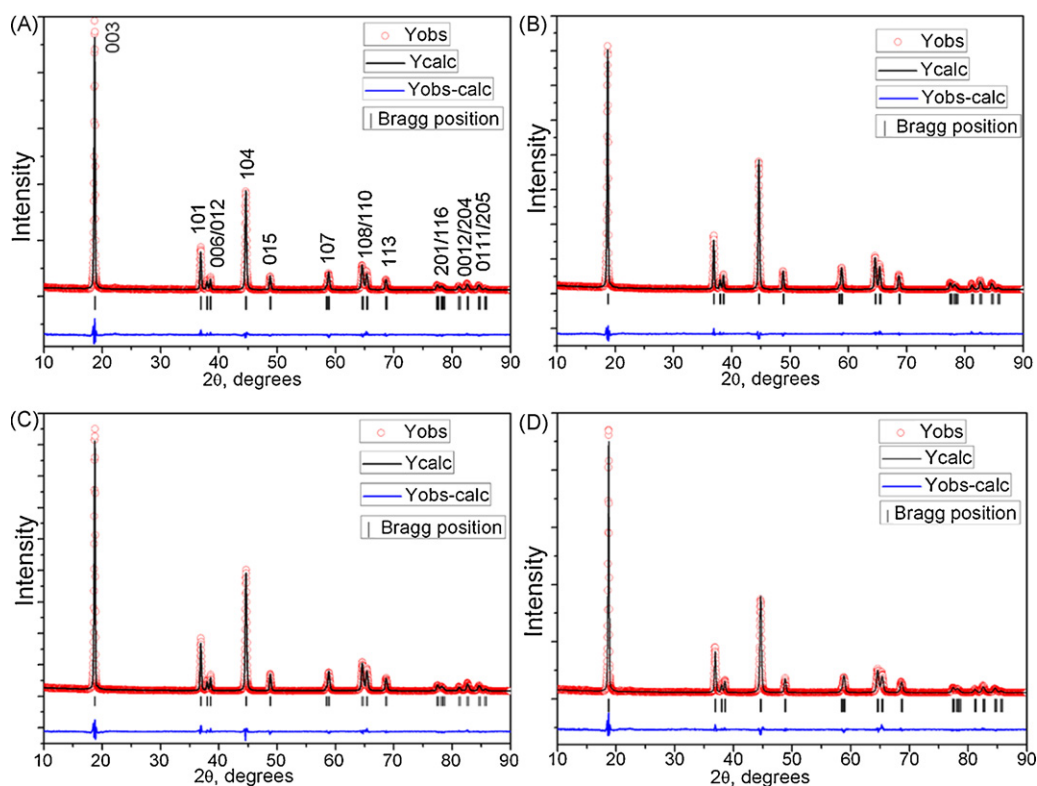


Fig. 3. Rietveld refinement results of X-ray diffraction patterns of $\text{LiNi}_{1/3}\text{Mn}_{1/3}\text{Co}_{1/3}\text{O}_2$ synthesized by different calcination time: (A) 4 h; (B) 6 h; (C) 8 h; (D) 10 h.

and $\text{Co}(\text{OH})_2$. The XRD patterns of the sample B is similar to other reports [9,16].

Fig. 2 shows SEM images of the $[\text{Ni}_{1/3}\text{Mn}_{1/3}\text{Co}_{1/3}](\text{OH})_2$ before and after hydrothermal treatment with $\text{LiOH}\cdot\text{H}_2\text{O}$. There is an evident distinction in morphology between the two precursors. The precursors A are composed of small layered particles (100–300 nm) which are greatly agglomerate. After hydrothermal treatment, rock-shaped grains with sharp edges morphology are formed, and the grain size increases to 200–400 nm. When the images are magnified to 10,000 times, it is clearly to see that the distribution of the particles is much more uniform after hydrothermal treatment. It is well known that particle shape and size of cathode materials can affect the energy density in practical use, so controlling particle morphology is very important [17].

The Rietveld method was performed to refine the crystal structure of the $\text{LiNi}_{1/3}\text{Mn}_{1/3}\text{Co}_{1/3}\text{O}_2$ prepared by different calcination time. The resulting Rietveld refinement pattern and the resultant parameters are shown in Fig. 3 and Table 1, respectively. The figure reveals there are no other impurity phases are observed. All peaks are sharp and well defined, suggesting that compounds are generally well crystallized. In the XRD pattern, integrated peak splits of (006)/(102) and (108)/(110) are indicators of characteristic of layer structure [18]. As seen from Fig. 3, regardless of short calcination time, the clearly peak splits of (006)/(102) and (108)/(110) observed in all the XRD patterns which indicate the layered $\text{LiNi}_{1/3}\text{Mn}_{1/3}\text{Co}_{1/3}\text{O}_2$ materials are successfully synthesized

by all the calcination time in this experiment. These results could be interpreted that homogeneous precursor obtained by hydrothermal treatment can be readily synthesized the layered compound even by short calcination time of 4 h. As shown in Table 1, the intensity ratio of the (003) to (104) lines is sensitive to the degree of cation mixing, in which the larger $I_{(003)}/I_{(104)}$ ratio indicates the less cation mixing between Li and Ni ions. Generally, when $I_{(003)}/I_{(104)} > 1.2$, the cation mixing is small [16]. The $I_{(003)}/I_{(104)}$ values of all the samples are larger than 1.2, this indicating less undesirable cation mixing takes place. The Rietveld refinements were carried out assuming a $\alpha\text{-NaFeO}_2$ type hexagonal structure ($R\bar{3}m$), in which Li ions occupy the 3b site; Ni, Mn and Co are located in the 3a site, and O is located in the 6c site. From Table 1, it is clearly to see that the sample B has the smallest Bragg R -factor (1.81%), which means a very good fit between the observed and calculated patterns. Therefore, we consider that the sample B in this study has the best $O3$ hexagonal structure [2]. c/a ratios of all the samples are greater than 4.9, a value is well known for the material with layered characteristics. The c/a ratio of the sample B is the largest, which means it has the highest layer properties and lowest cation mixing [2,19]. These results indicate the sample B has the best hexagonal ordering and excellent electrochemical performance.

The SEM images of the prepared $\text{LiNi}_{1/3}\text{Mn}_{1/3}\text{Co}_{1/3}\text{O}_2$ materials are presented in Fig. 4. It can be seen that there is no significant morphology difference of the synthesized materials. The average particle size of $\text{LiNi}_{1/3}\text{Mn}_{1/3}\text{Co}_{1/3}\text{O}_2$ is 300–500 nm, which is bigger

Table 1

Comparison of lattice parameters of the $\text{LiNi}_{1/3}\text{Mn}_{1/3}\text{Co}_{1/3}\text{O}_2$ powders synthesized by different calcination time: (A) 4 h; (B) 6 h; (C) 8 h; (D) 10 h.

Sample	a (Å)	c (Å)	c/a	I_{003}/I_{104}	R_{wp} (%)	R_{Bragg} (%)
A	2.85498(9)	14.21639(40)	4.979506	2.1890	11.8	3.09
B	2.85373(6)	14.21053(28)	4.979634	1.4436	8.77	1.81
C	2.85386(7)	14.21099(32)	4.979568	1.4456	10.8	2.47
D	2.85575(9)	14.21615(43)	4.978079	2.4372	11.8	3.07

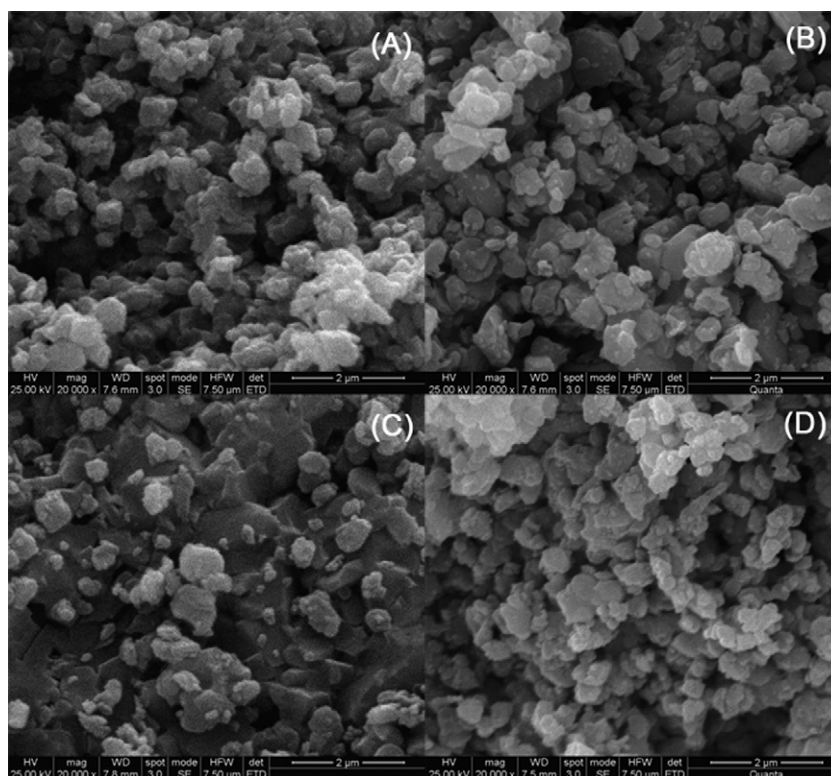


Fig. 4. SEM images of $\text{LiNi}_{1/3}\text{Mn}_{1/3}\text{Co}_{1/3}\text{O}_2$ synthesized by different calcination time: (A) 4 h; (B) 6 h; (C) 8 h; (D) 10 h.

than that of $[\text{Ni}_{1/3}\text{Mn}_{1/3}\text{Co}_{1/3}](\text{OH})_2$ (Fig. 2b). Table 2 is the result of energy dispersive X-ray (EDX) analysis for the sample B. The intensity values of each element are converted into weight and atomic percent. The atomic ratio of Ni, Mn and Co content in the powder is approximately 1/3, 1/3 and 1/3, respectively, which is almost the same as the mole ratio of the starting materials.

3.2. Electrochemical behavior

The initial charge–discharge curves of the prepared $\text{LiNi}_{1/3}\text{Mn}_{1/3}\text{Co}_{1/3}\text{O}_2$ between 2.8 and 4.5 V under a current density of 20 mA g^{-1} are showed in Fig. 5. The sample A calcined by 4 h shows an initial charge capacity of 223.8 mAh g^{-1} and discharge capacity of 160.6 mAh g^{-1} . On increasing calcination time to 6, 8 and 10 h, obtained discharge capacities are increased to 187.7, 175.5 and 158.1 mAh g^{-1} , respectively. The highest initial discharge capacity of 187.7 mAh g^{-1} is obtained by the sample B. The irreversible capacity loss of samples A, B, C and D are 28.2, 16.0, 19.5 and 17.5%, respectively. The smallest irreversible capacity loss of 16.0% is also obtained by the sample B. Thereafter, heat treatment for 6 h is the best time in this experiment. It indicates that 4 h is not enough for sufficient reaction to synthesize a high quality layered $\text{LiNi}_{1/3}\text{Mn}_{1/3}\text{Co}_{1/3}\text{O}_2$; 8 and 10 h are a little longer to obtained well behaved $\text{LiNi}_{1/3}\text{Mn}_{1/3}\text{Co}_{1/3}\text{O}_2$. The sample B has highest operation voltage would be ascribed to the improved structural integrity by the heat treatment. The irreversible capac-

ity loss is mainly attributed to the electrolyte decomposition and the formation of a solid electrolyte interface (SEI) on the surface of cathode materials during the first cycle [13]. One of the great merits of the hydrothermal treatment of hydroxides is it could greatly decrease the calcination temperature and time. The $\text{LiNi}_{1/3}\text{Mn}_{1/3}\text{Co}_{1/3}\text{O}_2$ obtained by traditional hydroxide coprecipitation method by other reports has to be heated at 1000°C for more than 10 h [9,20,21]. The discharge capacity obtained by Lee et al. [9] is 177.0 mAh g^{-1} . It could see that, the calcination temperature and time is not only much lower in our report but also the discharge capacity is higher.

The influence of calcination time on the cycling performance of $\text{LiNi}_{1/3}\text{Mn}_{1/3}\text{Co}_{1/3}\text{O}_2$ is also investigated. The cycling performance

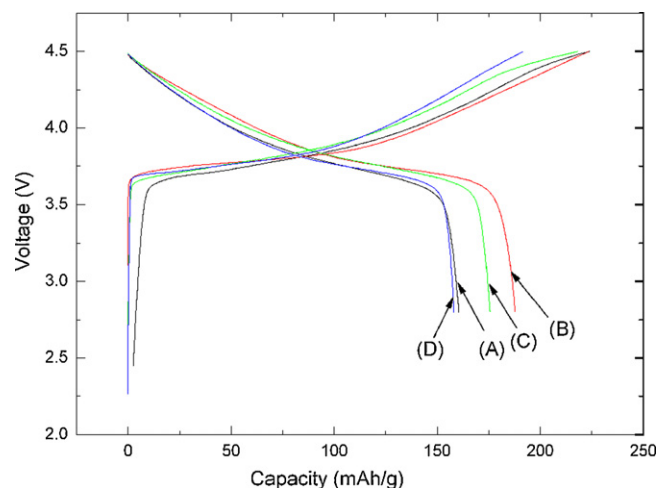


Fig. 5. The initial charge–discharge curves of $\text{LiNi}_{1/3}\text{Mn}_{1/3}\text{Co}_{1/3}\text{O}_2$ cells at 20 mA g^{-1} synthesized by different calcination time: (A) 4 h; (B) 6 h; (C) 8 h; (D) 10 h.

Table 2
EDX analysis data for sample B.

	Elements		
	Ni	Co	Mn
wt.%	26.24	26.02	24.16
at.%	15.95	15.76	15.70

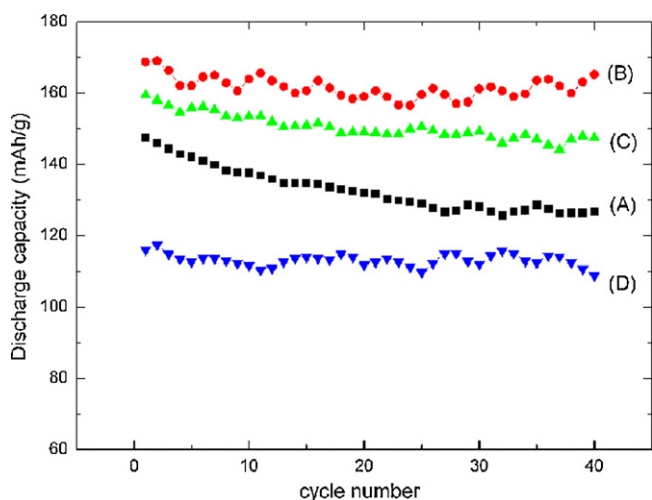


Fig. 6. The comparison of cycling performance for $\text{LiNi}_{1/3}\text{Mn}_{1/3}\text{Co}_{1/3}\text{O}_2$ prepared by different calcination time: (A) 4 h; (B) 6 h; (C) 8 h; (D) 10 h.

at 1.0C current is presented in the Fig. 6. The $\text{LiNi}_{1/3}\text{Mn}_{1/3}\text{Co}_{1/3}\text{O}_2$ calcined by 4, 6, 8 and 10 h delivered an initial discharge capacity of 147.4, 168.7, 159.4 and 116.0 mAh g^{-1} , respectively; the capacity retention of each sample after 40 cycles is 85.9, 97.9, 92.5 and 93.8%, respectively. Among all the samples, sample B has the highest discharge capacity and best cycling performance. These results are consistent with the XRD results in which the sample B has the lowest R -value of 0.4146. The performance of the sample B is much better than that of Luo et al. [17] reported which the capacity of 154.1 mAh g^{-1} was obtained at the end of 30th cycle with the retention of 93%. It can be considered that 6 h is the best calcination time by the hydrothermal method. The high discharge capacity and stable cycling performance of the prepared $\text{LiNi}_{1/3}\text{Mn}_{1/3}\text{Co}_{1/3}\text{O}_2$ could be attributed to its well-defined structure. As discussed above, the highly ordered layered structure and low amount of cation mixing prepared by this method are favorable to the electrochemical performance.

Fig. 7 presents the rate capabilities of the $\text{LiNi}_{1/3}\text{Mn}_{1/3}\text{Co}_{1/3}\text{O}_2$. The cells were charged to 4.5 V at 0.2 C, and then discharged to 2.8 V at 0.2, 1.0, 2.0, 3.0, 4.0 and 5.0 C, respectively. Obviously, as the current density increases, the discharge capacity of all the samples decreases due to polarization [22]. However, the sample B shows the best rate performance of 160.7 and 142.2 mAh g^{-1} at 2.0 and

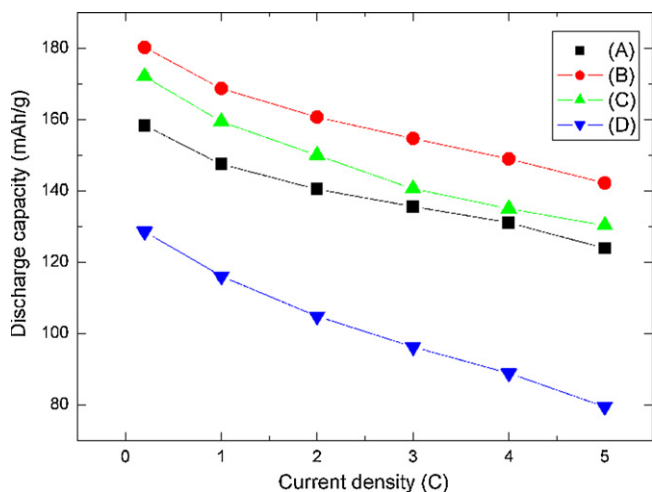


Fig. 7. Rate capability of $\text{LiNi}_{1/3}\text{Mn}_{1/3}\text{Co}_{1/3}\text{O}_2$ cells prepared by different calcination time: (A) 4 h; (B) 6 h; (C) 8 h; (D) 10 h.

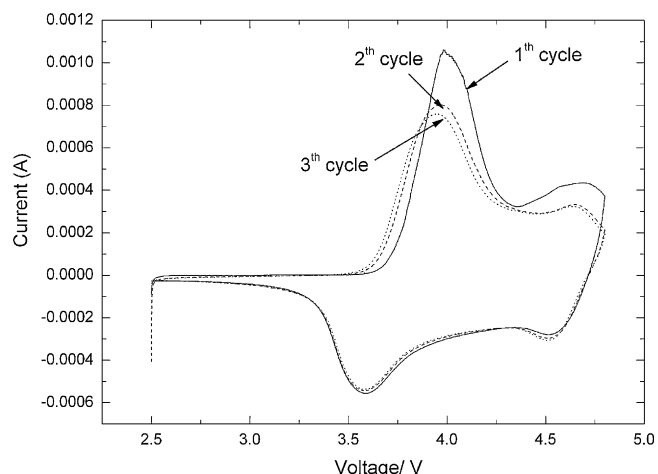


Fig. 8. Cyclic voltammetry of sample B between 2.5 and 4.8 V at a scan rate of 0.1 mV s^{-1} .

5.0 C, remaining 89.2 and 78.9% of the capacity of 180.2 mAh g^{-1} at the 0.2 C. The improved rate capability of the sample B could also be attributed to the enhanced stabilized structure.

3.3. Cyclic voltammetry (CV)

Cyclic voltammetry of the sample B (calcination for 6 h) between 2.5 and 4.8 V at a scan rate of 0.1 mV s^{-1} for the first three cycles are shown in Fig. 8. It could see that the first cycle anodic peaks center at 3.99 and 4.71 V which correspond to the $\text{Ni}^{2+}/\text{Ni}^{4+}$ and $\text{Co}^{3+}/\text{Co}^{4+}$ [6]. The cathodic peaks center at 3.58 and 4.54 V. Moreover, it is noted that no reduction peak near 3.2 V, this means there is no reduction of $\text{Mn}^{3+}/\text{Mn}^{4+}$ [23,24]. It is evident that the major anodic peak centers at 3.99 V in the first anodic scan shifts to lower voltage 3.96 V with slightly lower intensity and keep steadily during consequently scans, whereas its corresponding cathodic peak centers at 3.58 V in the first cathodic scan is not evidently shifted in position and intensity during the scans. After the first cycle, the curves of the second and third cycle almost overlap. This indicates the good reversible (de-)intercalation of Li ions in the synthesized $\text{LiNi}_{1/3}\text{Mn}_{1/3}\text{Co}_{1/3}\text{O}_2$. The redox peak at 4.71 V has the similar behavior, and the first anodic and cathodic peaks exhibited marked fading in intensity compared to the second and third scans. This fading in peak intensity may be partially attributed to the degradation between the first and consequent cycles. There are no obvious redox peak changes after the first cycle. This behavior implies that structural degradation is not expected during the lithium extraction/insertion process of $\text{LiNi}_{1/3}\text{Mn}_{1/3}\text{Co}_{1/3}\text{O}_2$.

3.4. Electrochemical impedance spectroscopy measurements

Fig. 9 compares the EIS profiles of the $\text{LiNi}_{1/3}\text{Mn}_{1/3}\text{Co}_{1/3}\text{O}_2$ before and after 40 cycles at 1.0 C. It could see that a single semi-circle appears at a high-frequency measured resistance of 74.4Ω (calculated from the first semicircle's diameter) for the freshly assembled cell which is followed by an inclined straight line. In general, the high-frequency semicircle reflects the impedance (R_{SEI}) due to a surface film forms on the surface of electrodes, i.e. the so-called solid electrolyte interface (SEI). The low-frequency tail is associates with the diffusion effects of Li-ion on the interface between the active material particles and electrolyte, which is called Warburg diffusion [25–28]. After 40 cycles, a new depressed semicircle appears in the relatively low-frequency region. This low-frequency semicircle is related to a slow charge transfer process at the interface and its relative double-layer capacitance

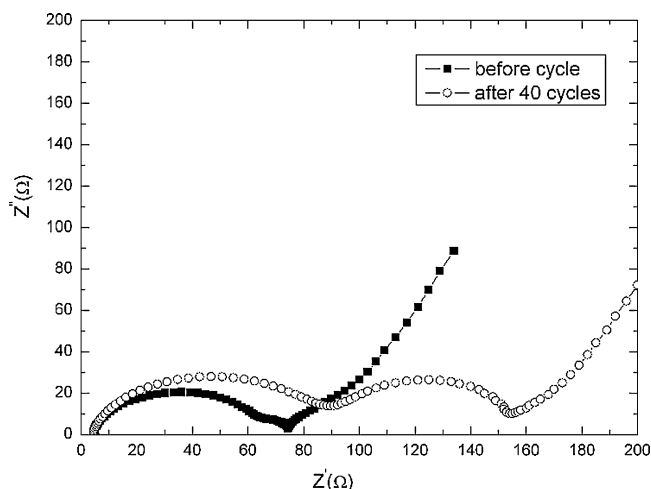
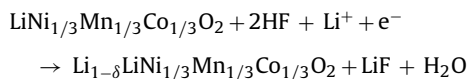


Fig. 9. Impedance spectra (Z'' vs. Z') of sample B.

at the film/bulk oxide and the numerical value of the semicircle diameter on the Z' axis is approximately equal to the charge transfer resistance (R_{ct}) [4]. It can be seen that the R_{SEI} value for the fresh electrode is increases to 88.9 Ω after 40 cycles, which means that an SEI film has been performed upon the contact of electrode and electrolyte. During cycling, the R_{ct} of the electrode increases to 65.4 Ω . The increase in the surface resistance of $\text{LiNi}_{1/3}\text{Mn}_{1/3}\text{Co}_{1/3}\text{O}_2$ is related to the $\text{LiNi}_{1/3}\text{Mn}_{1/3}\text{Co}_{1/3}\text{O}_2$ particles become slightly coarse after cycling. According to Markovsky [29], cathode material could be decomposed by HF attack from the electrolyte, which is generated by the decomposition of the electrolytic salt. $\text{LiNi}_{1/3}\text{Mn}_{1/3}\text{Co}_{1/3}\text{O}_2$ could be decomposed by the following reaction:



Moreover, polycarbonates, polymeric hydrocarbons, NiO-type phase, MnCO_3 , Li_2CO_3 , Li_xPF_y , $\text{Li}_x\text{PF}_y\text{O}_z$, NiF_2 , CoF_2 , and MnF_2 could also form on the surface of Li–Ni–Mn–Co–O compounds during cycling [4,27,30]. These byproducts could increase the resistance of the surface film and thereby dynamically hinder the movement of the lithium ions during the deintercalation/intercalation process. Due to the bare material directly exposed to HF, decomposition of $\text{LiNi}_{1/3}\text{Mn}_{1/3}\text{Co}_{1/3}\text{O}_2$ and the formation of byproducts occur much rapidly. Simultaneously, byproducts would attribute to increase in the internal resistance of the material because they are electrical insulator. This leads to the fast of capacity fade and increment of impedance for the bare material. The EIS phenomena might be able to explain part of the rate capability and the cycle life characteristics of the material. The increase in R_{SEI} and R_{ct} will cause a high cell polarization, leading to an apparent capacity loss.

4. Conclusions

The most highlighted point of this work is to synthesis $\text{LiNi}_{1/3}\text{Mn}_{1/3}\text{Co}_{1/3}\text{O}_2$ by treat the $[\text{Ni}_{1/3}\text{Mn}_{1/3}\text{Co}_{1/3}](\text{OH})_2$ precur-

sor with excess amount of LiOH aqueous solution at 160 $^\circ\text{C}$ by the hydrothermal method. This method could lower the final calcination temperature and shorten calcination time. The XRD patterns reveal that $\text{LiNi}_{1/3}\text{Mn}_{1/3}\text{Co}_{1/3}\text{O}_2$ could be synthesized even by short calcination time of 4 h. The $\text{LiNi}_{1/3}\text{Mn}_{1/3}\text{Co}_{1/3}\text{O}_2$ calcined by 6 h exhibits the highest discharge capacity of 187.7 mAh g^{-1} at a current density of 20 mA g^{-1} and the capacity retention after 40 cycles at 1.0 C is 97.9%. The good electrochemical performance of $\text{LiNi}_{1/3}\text{Mn}_{1/3}\text{Co}_{1/3}\text{O}_2$ prepared by this method can be attributed to the highly ordered layered structure and low amount of cation mixing. It is concluded that this hydrothermal treatment is an excellent method to synthesize cathode material, which ultimately results in excellent performance of the final product $\text{LiNi}_{1/3}\text{Mn}_{1/3}\text{Co}_{1/3}\text{O}_2$.

Acknowledgements

This work was financially supported by the National 973 program (Contact Nos. 2002CB211800 and 2009CB220100), National High-tech 863 key program (Contact No. 2006AA11A165) and BIT Basic Research Fund (Contact No. 20070542004).

References

- [1] Y.-K. Sun, S.-T. Myung, M.-H. Kim, J. Prakash, K. Amine, J. Am. Chem. Soc. 127 (2005) 13411.
- [2] S.W. Oh, S.H. Park, C.-W. Park, Y.-K. Sun, Solid State Ionics 171 (2004) 167.
- [3] P.Y. Liao, J.G. Duh, S.R. Sheen, J. Power Sources 143 (2005) 212.
- [4] S.-T. Myung, K. Izumi, S. Komaba, H. Yashiro, H.J. Bang, Y.-K. Sun, N. Kumagai, J. Phys. Chem. C 111 (2007) 4061.
- [5] T. Ohzuku, Y. Makimura, Chem. Lett. (2001) 642.
- [6] K.M. Shaju, G.V. Subba Rao, B.V.R. Chowdari, Electrochim. Acta 48 (2002) 145.
- [7] J.-M. Kim, H.-T. Chung, Electrochim. Acta 49 (2004) 3573.
- [8] S.H. Park, C.S. Yoon, S.G. Kang, H.-S. Kim, S.-I. Moon, Y.-K. Sun, Electrochim. Acta 49 (2004) 557.
- [9] M.-H. Lee, Y.-J. Kang, S.-T. Myung, Y.-K. Sun, Electrochim. Acta 50 (2004) 939.
- [10] C.H. Song, A. Manuel Stephan, A. Kim, K.S. Nahm, J. Electrochem. Soc. 153 (2006) A390.
- [11] H. Huang, P.G. Bruce, J. Electrochem. Soc. 141 (1994) L106.
- [12] T. Nukuda, T. Inamasu, A. Fujii, D. Endo, H. Nakagawa, S. Kozono, T. Iguchi, J. Kuratomi, K. Kohno, S. Izuchi, M. Oshitani, J. Power Sources 146 (2005) 611.
- [13] Z. Wang, Y. Sun, L. Chen, X. Huang, J. Electrochem. Soc. 151 (2004) A914.
- [14] S. Patoux, M.M. Doeff, Electrochem. Commun. 6 (2004) 767.
- [15] S.T. Myung, S. Komaba, N. Kumagai, Solid State Ionics 150 (2002) 199.
- [16] X. Luo, X. Wang, L. Liao, X. Wang, S. Gamboa, P.J. Sebastian, J. Power Sources 161 (2006) 601.
- [17] X. Luo, X. Wang, L. Liao, S. Gamboa, P.J. Sebastian, J. Power Sources 158 (2006) 654.
- [18] A. Rougier, P. Gravereau, C. Delmas, J. Electrochem. Soc. 143 (1996) 1168.
- [19] Y.M. Choi, S. Ilpyun, S.I. Moon, Solid State Ionics 89 (1996) 43.
- [20] N. Yabuuchi, Y. Makimura, T. Ohzuku, J. Electrochem. Soc. 154 (2007) A314.
- [21] N. Yabuuchi, Y. Koyama, N. Nakayama, T. Ohzuku, J. Electrochem. Soc. 152 (2005) A1434.
- [22] Y. Kim, H.S. Kim, S.W. Martin, Electrochim. Acta 52 (2006) 1316.
- [23] S. Gopukumar, K.Y. Chung, K.B. Kim, Electrochim. Acta 49 (2004) 803.
- [24] C. Gan, X. Hu, H. Zhan, Y. Zhou, Solid State Ionics 176 (2005) 687.
- [25] H.-W. Ha, N.J. Yun, K. Kim, Electrochim. Acta 52 (2007) 3236.
- [26] H.-S. Kim, M. Kong, K. Kim, I.-J. Kim, H.-B. Gu, J. Power Sources 171 (2007) 917.
- [27] Z.R. Zhang, H.S. Liu, Z.L. Gong, Y. Yang, J. Power Sources 129 (2004) 101.
- [28] Q. Cao, H.P. Zhang, G.J. Zhang, Q. Xia, Y.P. Wu, H.Q. Wu, Electrochem. Commun. 9 (2007) 1228.
- [29] B. Markovsky, A. Rodkin, G. Salitra, Y. Talyosef, D. Aurbach, H.-J. Kim, J. Electrochem. Soc. 151 (2004) A1068.
- [30] I. Belharouak, W. Lu, D. Vissers, K. Amine, Electrochem. Commun. 8 (2006) 329.